The Toroidal Volcanic Reservoir of Tofua Volcano, a Possible Predecessor of the Hunga Tonga Present Structure

Román Alvarez[1,*], Miguel Camacho[2]

[1]Applied Mathematics and Systems Research Institute, National Autonomous University of Mexico, Mexico City 04510, Mexico

[2]Department of Earth Sciences, National Autonomous University of Mexico, Mexico City 04510, Mexico

Abstract: The recent, powerful outburst of the Hunga Tonga Hunga Ha'apai (HTHH) volcano gave rise to various phenomena, some of which are in the process of explanation; an important one that has not yet been resolved is the volcanic mechanism that gave rise to the unusually strong eruption. In an attempt at identifying precursors of this type of explosion, we looked into volcanic structures in the same region, with characteristics similar to the HTHH structure. Tofua volcano is located in the Tonga volcanic arc, its structure emerges from the sea forming an island; it experienced explosive volcanism estimated at ~3 ka. Ring fractures and failure of the magma deposit's roof induced the stratovolcano's collapse and the caldera formation. Using high-resolution, satellite-derived gravity data we explore its interior to determine the present distribution of materials; with the complete Bouguer Anomaly of the area we perform 3-D gravity inversions to acquire density distributions. We located a toroidal, low-density deposit linked to the ring fractures developed previous to the stratovolcano's collapse. The toroidal deposit delimits the perimeter of the collapsed region. Since we formerly inferred a similar ring fracture zone in the structure of the Hunga Tonga volcano, we speculate that a similar toroidal deposit may have existed before its January 15, 2022, violent eruption, giving rise to the unusual dispersion of surficial, low-density regions detected in it.

Keywords: Tofua Volcano; Hunga Tonga-Hunga Ha'apai Volcano; Bouguer Anomaly; Ring Fractures; Tonga-Kermadec Island Arc

DOI: 10.57237/j.earth.2024.01.001

1 Introduction

Cataclysmic volcanic eruptions are unusual and involve phenomena concerning various disciplines in the Earth Sciences; when they occur in volcanic structures under the ocean the interaction of magmatic products with seawater creates powerful disturbances not only affecting the ocean but also the atmosphere and the stratosphere. The most recent eruption of this type occurred in one of the structures of the Tonga-Kermadec volcanic arc: the Hunga Tonga-Hunga Ha'apai volcano (HTHH) on January 15, 2022. Determining the conditions of the volcano prior to the eruption is of major interest, not only to help anticipate future similar eruptions but also to understand the mechanisms involved in the interaction of magma products and seawater.

The objective of the present work is to explore volcanic structures in the Tonga-Kermadec volcanic arc with conditions similar to those observed in the HTHH volcano, since the mechanisms that led to the powerful eruption are

*Corresponding author: Román Alvarez, roman.alvarez@iimas.unam.mx

Received: 4 November 2024; Accepted: 30 December 2024; Published Online: 9 January 2025 http://www.earthscieng.com

not clearly established. As a first case, we selected Tofua volcano, with geologic studies describing its structure and also presenting caldera collapse. The methodology we use to look at its internal structure consists of performing 3D gravity inversions to obtain density distributions.

When a magma chamber feeding a volcano gets depleted, the upward pressure sustaining the roof of the chamber decreases and, under certain circumstances, the roof and the volcanic structure above, collapse. Scandone and Lipman analyzed the conditions under which subsidence and collapse occur in volcanic calderas [26, 32]. Studying the characteristics of caldera collapse during ignimbrite eruptions it was concluded that a ring fault develops towards the surface of the volcanic structure, induced by overpressure of the roof of the magma chamber [31]. The model proposed in [9] for the formation of the caldera of Tofua Volcano includes the development of ring faults. Until now, no physical evidence has been provided for their existence.

Two examples of underwater stratovolcanoes that have experienced collapses and caldera formation are the HTHH volcano and the the Tofua volcano, located in the central Tonga arc (Figure 1), both have lost their upper structures owing to caldera collapse [9, 15, 38]. Tectonic and magmatic models for developing the Tonga-Kermadec volcanic arc were presented [36], the geologic characteristics of Tofua Volcano were also reported [6], as well as the geology, petrography, and geochemistry of the volcanic islands of Tonga [7]; however, the powerful eruption of HTHH on January 15, 2022, compelled additional information on the structure of this type of volcano. Some of the effects of this eruption are reported in [8, 38] regarding tsunamigenic aspects. In [40, 41] the authors reported about the seismic episodes originating in the volcano. Seismically induced stratospheric disturbances were reported [39] as well as their modeling [20, 22, 44].

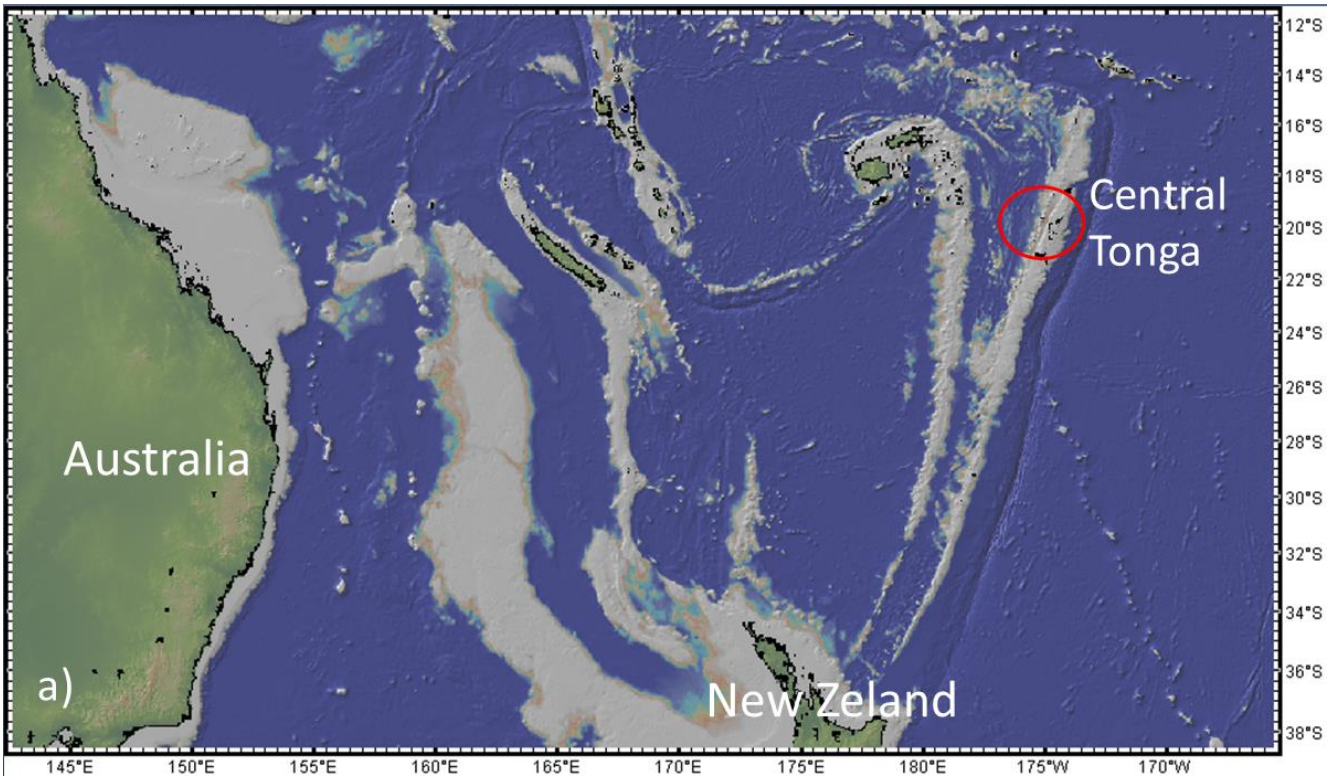

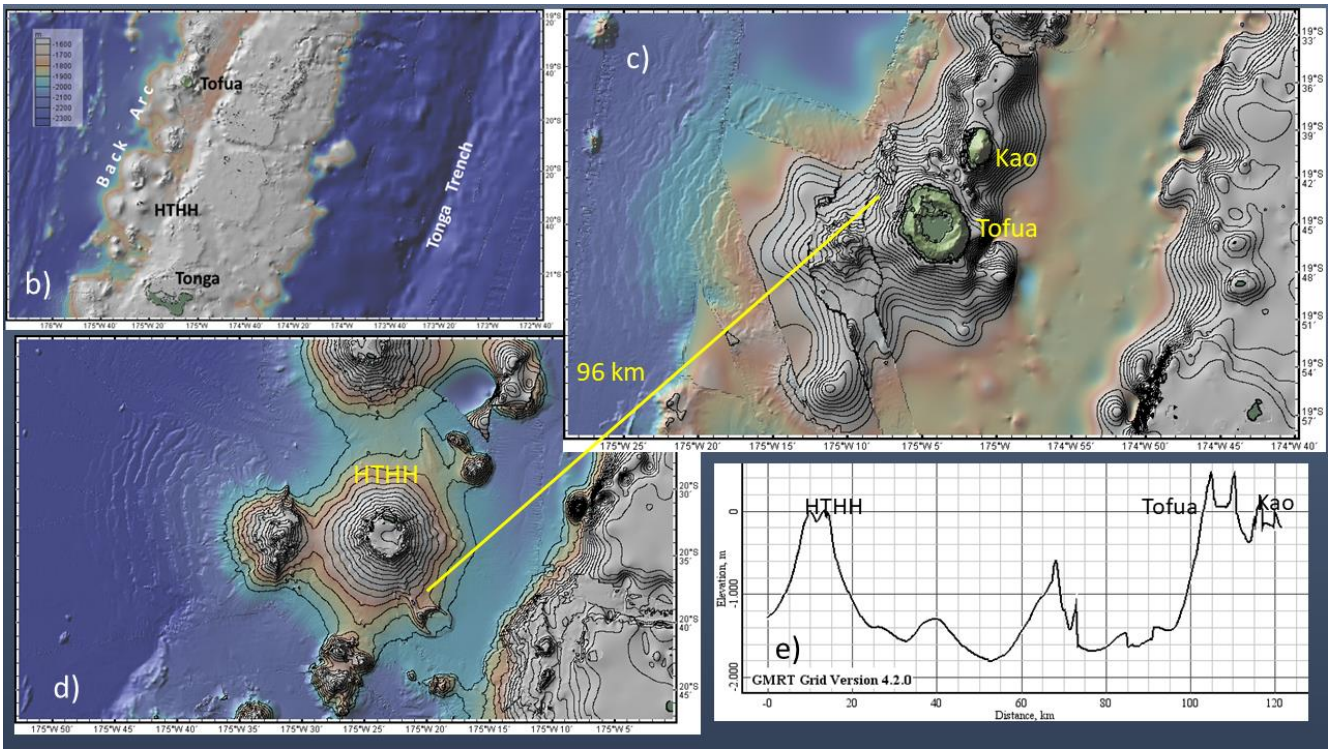

Figure 1 a) Location in the Pacific Ocean of the Central Tonga region. b) Location of the Back Arc and the Tonga Trench; the position of the HTHH and Tofua volcanoes is indicated. c) and d) Closer views of the HTHH and Tofua/Kao volcanoes. The regions protruding above sea level are shown in green tones. They can also be identified in the topographic profile along a line (not shown) that goes through the centers of these volcanic edifices. e) Topographic profile between HTHH and Tofua volcanoes; the distance between them is 96 km—maps from GeomapApp

The January 15, 2022 eruption of the HTHH Volcano injected about 10% of the water existing in the stratosphere [27]. Modeling the plumbing system of the HTHH Volcano with high-resolution, satellite-derived gravity data [19], no magma chamber was found in [2] within 6 km depth, instead, the authors located a disordered distribution of surficial, low-density pockets which they identified with deposits of magmatic material. They also identified two surface areas covering 12 and 14 km^2, potentially coming in contact with seawater, inducing the strong evaporation observed. In [2] were also able to identify inside HTHH volcano a surficial, circular structure that could be associated with the ring faults in the Tofua Volcano [9].

Analysis of the gravity of the HTHH volcano region was made [25] before and after the eruption on January 15, 2022, using satellite-derived gravity data [33, 34]; they reached a conclusion similar to that of [2], determining that there is a complex, multi-reservoir magma system in the volcano, with two main, low-density reservoirs., An example of another volcano fed by two reservoirs is the Ambrym volcano, in Vanuatu, reported in [24, 28].

The possibility was examined of magma transfer between two hydraulically connected magma lenses [35]. Looking at basaltic calderas, such as Kilauea [30], and Piton de la Fournaise [11], it was concluded that eruptive magma lays in isolated pockets at depths 1-6 km below the surface and up to 10 km away from the central caldera. This phenomenon may help explain the collective response of the magma pockets observed in the HTHH Volcano.

2 Materials and Methods

2.1 Satellite-derived Gravity

The calculation of gravity in the GGMplus model utilized here, is carried out by combining satellite, terrestrial, and topographic gravity data, using massive parallel computing techniques. First, the most recent gravity data measured by the GOCE and GRACE satellites are incorporated, providing information at spatial scales of ~10000 to ~100 km. Then, data from the EGM2008 model [18], which covers scales from ~100 to ~10 km in the geoid, are added [19]. Finally, terrestrial, airborne, and marine data from the EGM2008 model are integrated, combining

them with gravimetry calculated from high-resolution topographic models, using a technique called topographic gravity, which is derived from high-resolution terrain models and complements scales from ~10 km to ~250 m [17, 19]. This integrated approach allows for the generation of an ultra-high-resolution gravity model with a spatial precision of 7.2 arc-seconds (~200 m in the north-south direction), and an accuracy ranging from 2 to 5 mGal [19], although this depends on the quality of the topographic model in the area and the gravimetric data collected for the model. For example, in Africa, the average difference is usually 8 mGal compared to ground measurements.

Topographic gravity is based on a calculation with an assumed mass density of 2670 kg/m ^{3}and provides spatial scales from ~10 km to ~250 m. The conversion from topography to topographic gravity is performed using the residual terrain modeling technique [13], with high-frequency filtered topography through the subtraction of a spherical harmonic reference surface, of degree and order 2160, before direct modeling. In this procedure, large water masses are converted into equivalent rock layers using a combination of residual terrain modeling with the concept of equivalent rock topography [19]. These procedures generate short-scale topographic gravity that is suitable for extending spherical harmonic gravity models of degree 2190 beyond their associated resolution [19].

2.2 The Bouguer Anomaly

We obtained the high-resolution, satellite-derived data set GGMplus [19] corresponding to the Tofua/Kao volcanic area. The same data set was previously obtained for the location of the HTHH Volcano [2]. It is well known that this data set was acquired within a latitudinal belt that comprises the Earth's region between ±60 °; this belt contains a major oceanic region that is not fully processed. Fortunately, the areas corresponding to some islands are available in limited patterns, which is the case of the volcanic structures involved in this study. The process for obtaining the Bouguer Anomaly (BA) has been repeatedly described in various publications [1, 2, 4, 14]; we refer the reader to those publications.

We can summarize the procedure by saying that the raw dataset is obtained from http://ddfe.curtin.edu.au/gravitymodels/GGMplus/; using Gravity Observed ($G_{Obs)}$ from it, to calculate the BA according to the new gravimetric standard of the USGS [16]. The elevation at each point must be known; we used the topographic model with a resolution of ~450 m: https://download.gebco.net/ [42]. For the topographic correction, we employed the method implemented in the Oasis Montaj program of Geosoft, which uses the algorithm proposed by Kane [21] and supplemented by Nagy [29]. Gravimetry data were prepared for inversion through a Gaussian filter that separates the residual, to highlight the structures associated with volcanic edifices.

Negative gravity anomalies are often related to volcanic edifices associated with the presence of magma chambers and volcanic plumbing systems [1, 3, 14, 37].

2.3 General Characteristics of the BA

A general description of the characteristics of the BA associated with the Tofua volcano in Figure 2 begins with a description of its disk-like appearance in the vicinity of the intersection of lines S1 and S3. We note that the central portion of the anomaly has higher gravity values than its perimetral neighbors, which does not correspond to the traditional expectation of lower gravity values at the central volcano chimney [1, 3, 4, 14].

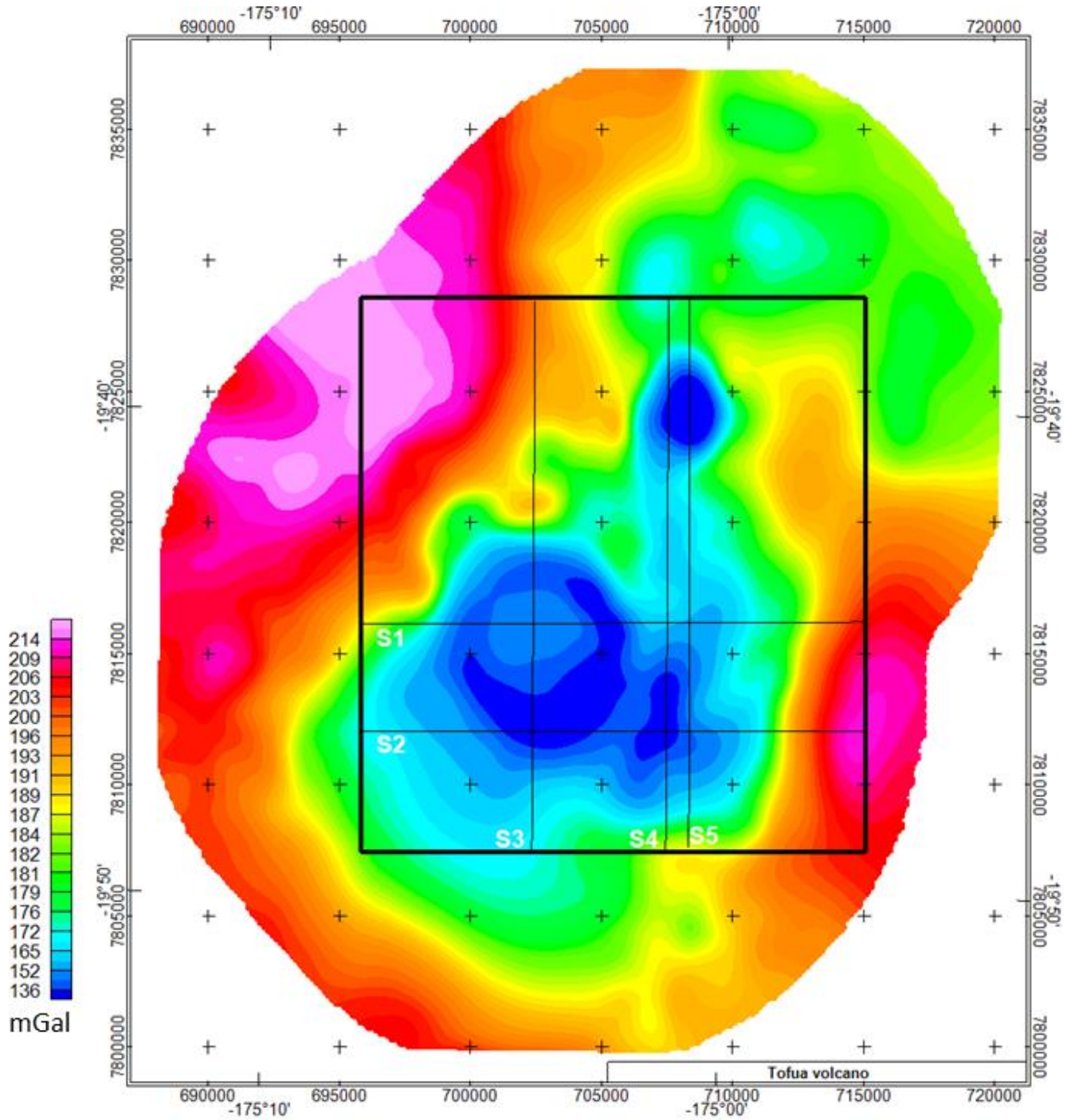

Figure 2 Complete Bouguer Anomaly of the Tofua and Kao volcanoes obtained from the GGMplus dataset. The main low-gravity anomaly corresponds to the former, while the smaller one to the NE belongs to the latter. A faint N-S-directed, low-gravity anomaly connects both. Lines labeled S1-S5 correspond to density cross-sections from the 3D, gravity-inverted model. The rectangle indicates the limits of the inverted region. The black, rectangular polygon corresponds to the 500 m resolution, 3D inversion. Lines S1-S5 correspond to the cross-sections to be presented below

2.4 3-D Inversion of the BA

The 3D inversion of the BA appears in Figure 3; the final density distribution reproduces the observed BA within 5 percent of the standard deviation of the data; the inversion resolution is 500 m, represented by the element cubes constituting the model.

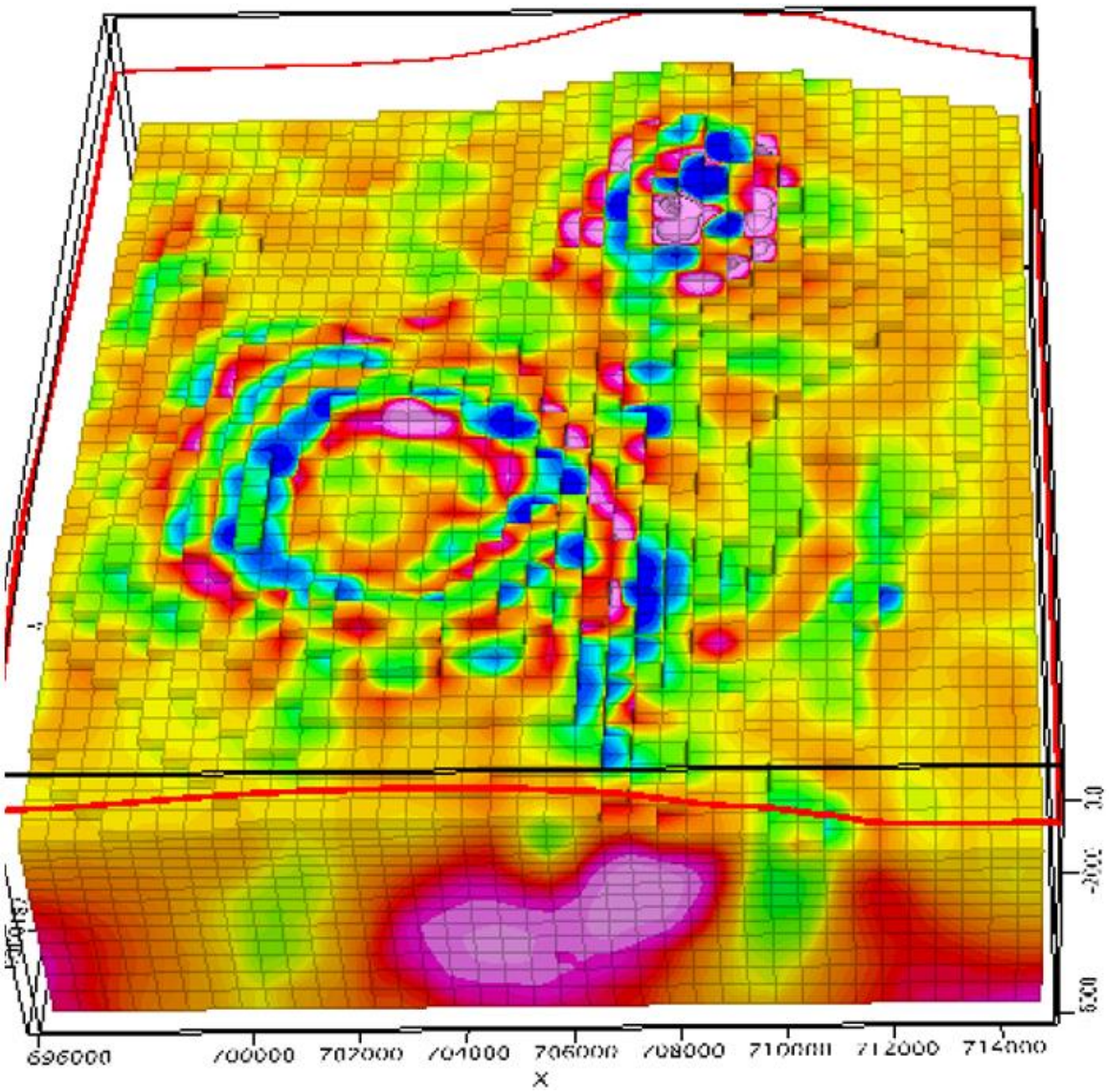

Figure 3 A 3D inversion of the region containing Tofua and Kao volcanoes showing the density distribution at 500 m resolution: In the case of Tofua, there is a concentric density distribution on the volcanic structure. The depth of the inverted volume is 6 km. Cross-sections are extracted from this density distribution to describe the volcanic characteristics at various locations and depths. Blue represents low-density regions; a color-density scale is presented with each cross-section

Horizontal cross-sections of this density distribution are extracted at depths ranging from -1650 to -6000 m (Figure 4) showing the existence of a circular, low-density region that appears in the -1650 and the -2000 m sections, not showing in the -3000 and the -6000 m horizontal sections.

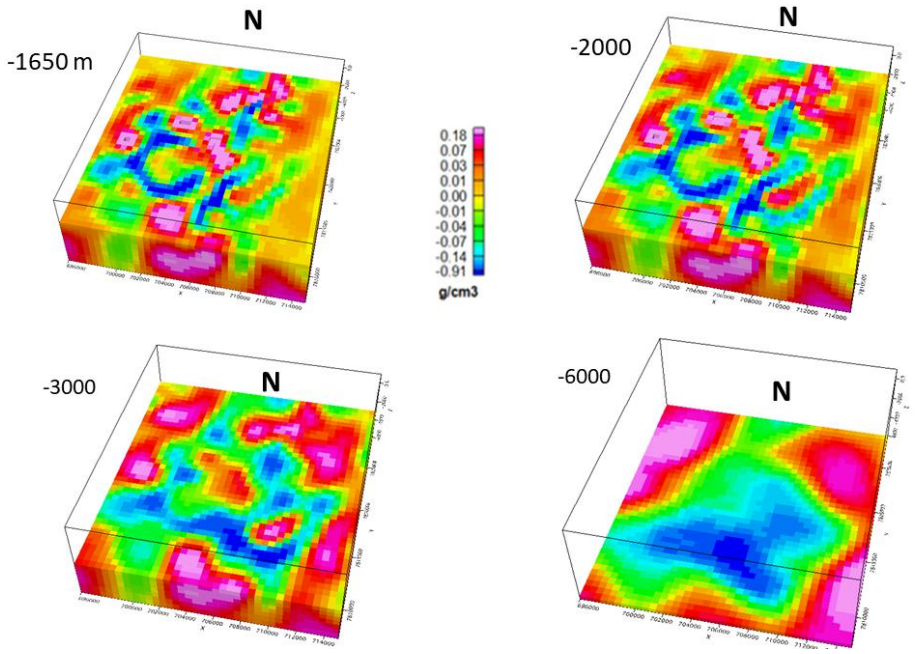

Figure 4 Depth evolution of the 3D density distribution from -1650 to -6000 m. A circular, low-density deposit is present in the -1650 and the -2000 m horizontal, density sections. The -6000 m horizontal section shows a region of minimum density that is probably the connection with a lower, feeding deposit. The color scale is valid for the four sections and the scale represents density contrast values relative to +2.67 g/cm^3

3 Results

3.1 The Isosurfaces

From the 3D inversion, we isolated the region with a density lower than 2.9 g/cm^3, represented by a blue surface delimiting it in Figure 5; it shows the isosurfaces enclosing density values lower than this one. Higher density values in the model are eliminated to allow for this description.

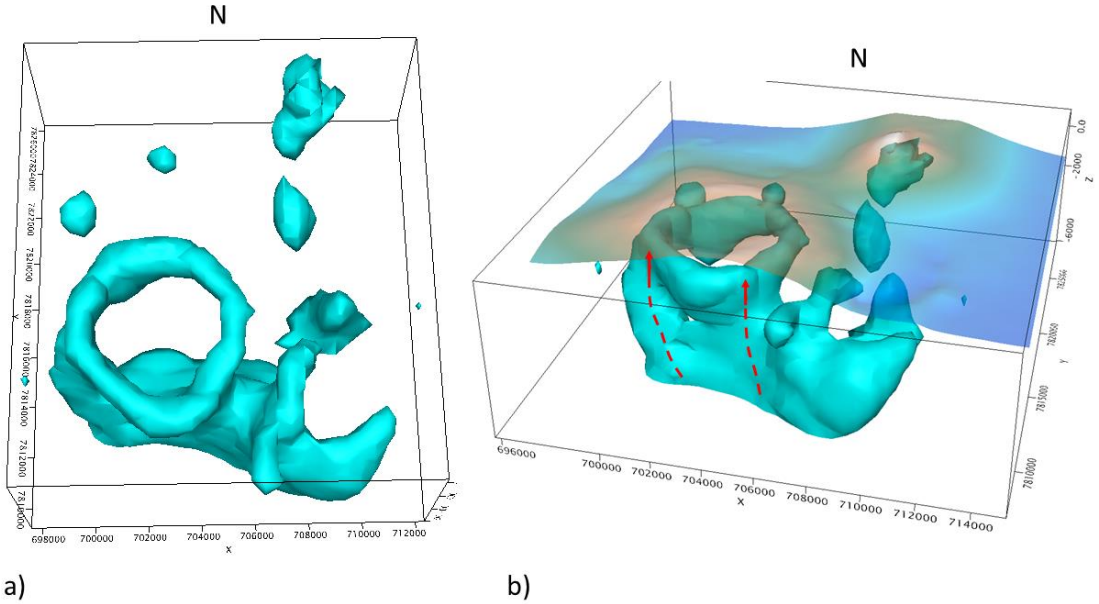

Figure 5 Density surfaces enclosing model densities ≤2.37 g/cm^3. a) Vertical view, showing the low-density toroidal deposit. b) Slanted view of the same distribution showing its deeper configuration; the bottom reaches 6 km in depth and the digital elevation model (DEM) is displayed with a selected degree of transparency. Feeding channels to the toroid are located on the W and SE sides of the distribution (red)

Contrary to expectations, this density distribution does not show a central conduit in the volcano, usually corresponding to its chimney, posing essential questions on the origin of this distribution. A model was proposed [9] in which an original strato-volcano collapsed after the extensive development of ring faults, and overpressure from a water-saturated dacite body located under 5 km depth, which created the overpressure and the ring fault formation, with the subsequent collapse of the structure. They also report two eruptions, one exhausting volcanic ash and ignimbrites around the rim of the central collapse, and the second, called the Hokula pyroclastic eruption, similarly on the rim of the collapsed portion. The conditions necessary for the occurrence of caldera collapse during ignimbrite eruptions were explored in [31]. A series of smaller-scale structures were identified in the northern fissure zone and concentric to the caldera faults, as conduits for magma eruption [5].

An estimate of the volume of the low-density materials contained in the torus can be obtained using the formula (1) for the volume V enclosed by a toroidal surface:

$$V = \pi r^2 \cdot 2\pi R \tag{1}$$

Where r is the radius of the cross-section of the torus, and R is the distance from the center of rotation of the cross-section to the center of the cross-section. Approximate values, for these parameters derived from the cross-sections, are r=1 km, and R=3 km, from which the value for the volume is 59 km^3.

3.2 The Cross-sections

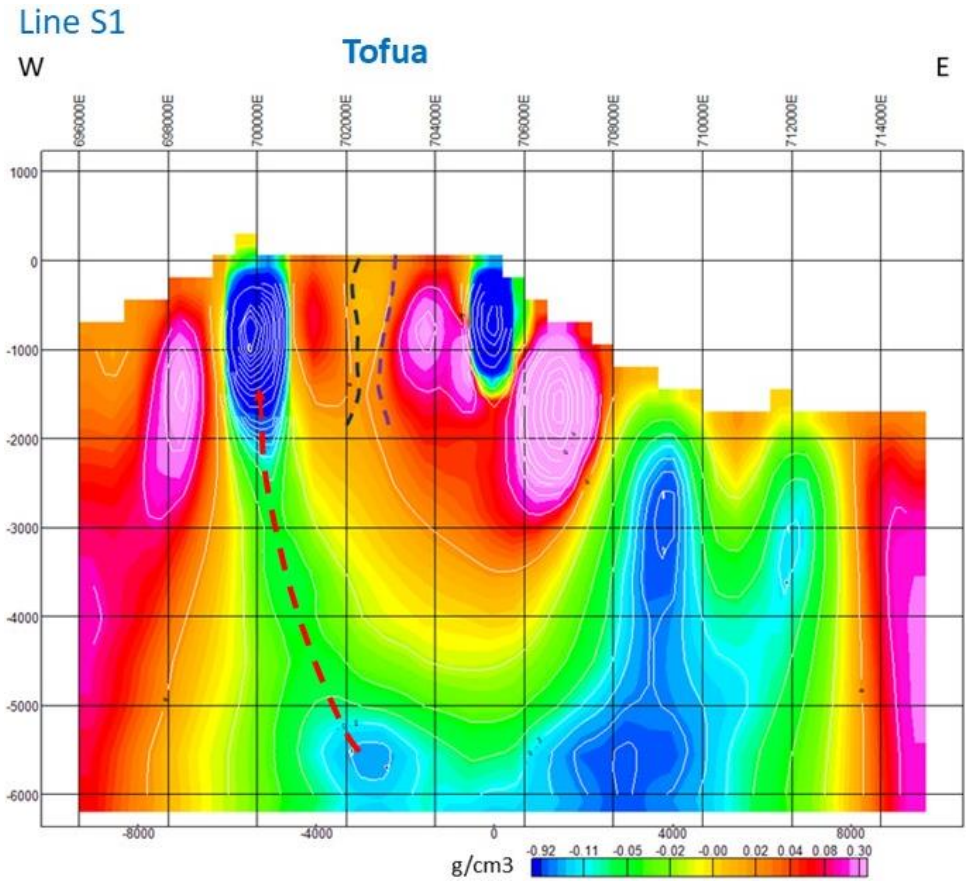

Figure 6 Cross-section S1 (Figure 2) extends along an E-W diameter of the circular structure, obtained from the 3D inversion in Figure 3, at 500 m resolution. The topographic profile of the volcano is recognized, and the intersections with the low-density torus are crossed just below the sea level; the western cross-section is about twice as deep as the eastern one. Between them, high-density regions represent the collapsed portion of the volcanic cone, where the former chimney is inferred as a lower-density region highlighted by dashed lines. Outside of the torus, high-density regions conform to the flanks of the volcanic structure. A dashed line on the west side indicates a low-density feeding path to the toroidal deposit. A vertical, low-density branch rises to the surface on the east side. The color scale represents density contrast values relative to +2.67 g/cm^3

Cross-section S1 (Figure 2) intersects the Tofua structure along a diameter of the circular structure. Figure 5 shows the density cross-section along S1, depicting the base of the original volcanic cone truncated above sea level; according to [9] the upper, conical section of the structure collapsed and sank into the central portion of the cone. This collapsed portion is represented here by the central, high-density region, where we infer with two dashed lines the location of the former volcanic chimney, identified as a lower-density gap within the collapsed section. The toroidal cross-sections flank the central, high-density region, presenting minima located at 750 mbsl, suggesting the concentration of eruptive volcanic materials around such locations. Two, high-density regions flank the outside of the toroidal region; we interpret them as part of the original volcanic edifice. Lateral deflection of the main feeding source is observed in several volcanic structures; here we see one such deflection on the E-side, with two minima, one located at -5.8 km and the other at -3 km, which are likely fed from the same, deeper source feeding Tofua volcano. Notice that the lowest density values occur within the toroidal structure.

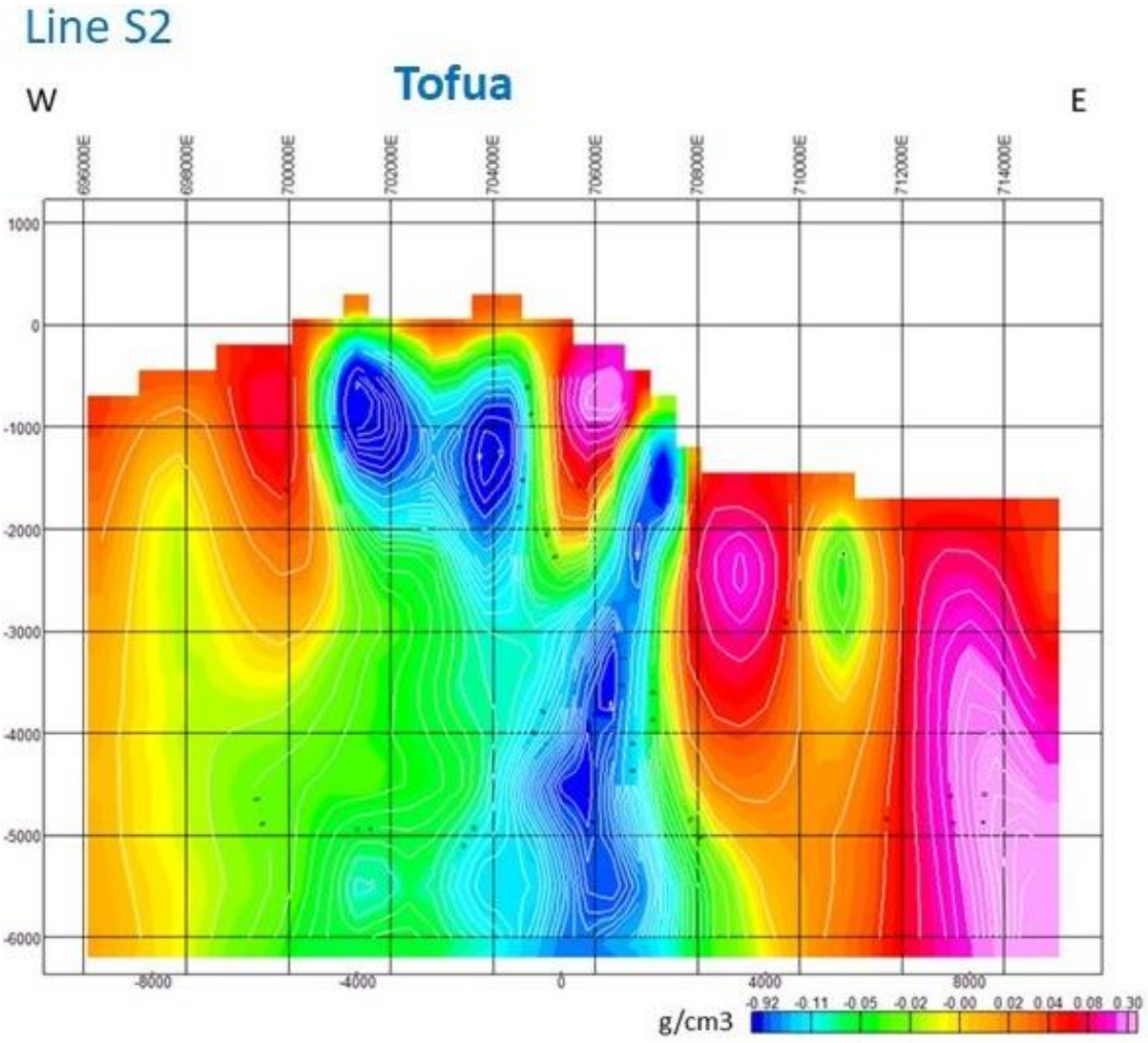

Figure 7 Cross-section S2 (Figure 2). This cross-section is also obtained from the 3D inversion (Figure 3); it intersects the torus south of S1 and adequately shows the closer positions of the toroidal cross-sections and the high-density regions flanking the volcanic structure. The vertical, low-density branch is more fully shown, rising to the surface on the east side. The caldera profile is delineated along this E-W cross-section The color scale represents density contrast values relative to +2.67 g/cm^3

Cross-section S2 (Figure 2) intersects the Tofua structure in the E-W direction, S of S1; the central collapsed region is not intersected, and the two regions of the toroidal volcanic deposit. Here, the toroidal cross-sections appear next to each other, and their lowest-density regions have minima at depths of -800 and -1300 m. What was identified as an eastern deflection of the feeding source, appears more clearly defined in this cross-section, where a feeding channel is observed from the bottom of the model (-6 km) to the base of the volcano (-1 km). A branching connection to the toroidal deposit occurs at -3 km, suggesting this is a feeding trajectory of magmatic materials.

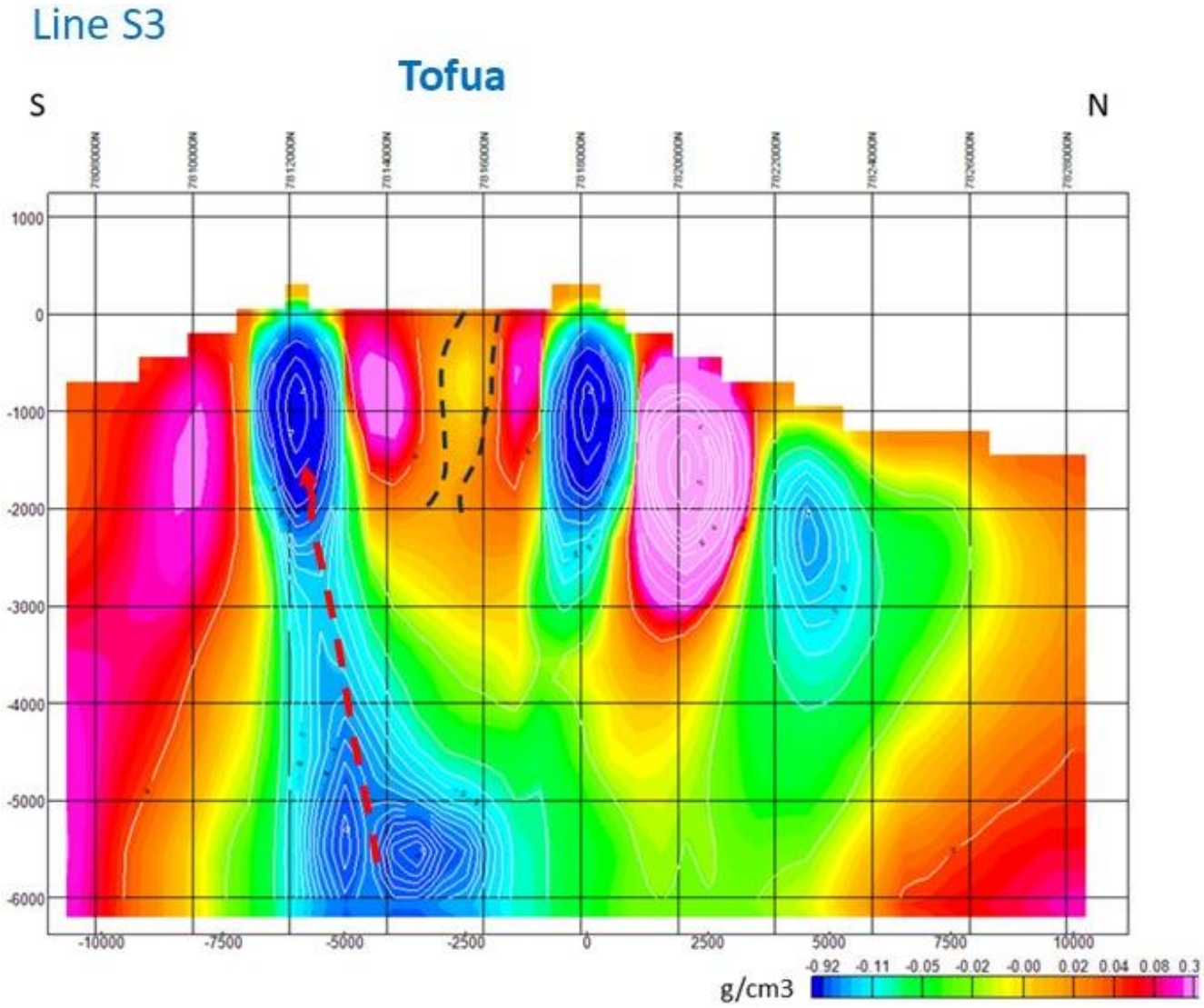

Figure 8 Cross-section S3 (Figure 2) extends along an N-S diameter of the circular structure, obtained from the 3D inversion in Figure 3; this cross-section is similar in structure to S1, confirming the circular geometry of the upper layers. A feeding channel appears now on the S portion, showing two deposits, with their respective centers at 5.5 km bsl, rising to the S section of the torus. The N portion shows another wide, region with intermediate density values approaching the volcano's surface. The caldera profile is delineated along this N-S cross-section. The color scale represents density contrast values relative to +2.67 g/cm^3

Cross-section S3 (Figure 2) intersects the Tofua structure in the N-S direction along a diameter; the result is similar to that obtained along line S1. The collapsed portion of the volcano appears as a high-density zone with the inferred chimney trajectory indicated by two dashed lines. The low-density distributions corresponding to the intersection with the toroidal deposit show a depth of 2 km, while their minima are at – 1 km. The central, collapsed portion is separated from the high-density region to the N by the toroidal section; in the case of S1, it

appeared directly connected to it. A deep, low-density section presents minima centered at -5.5 km; it appears to directly feed the southern portion of the toroidal volcanic deposit. The 3D views in Figure 4 confirm the connection along this location.

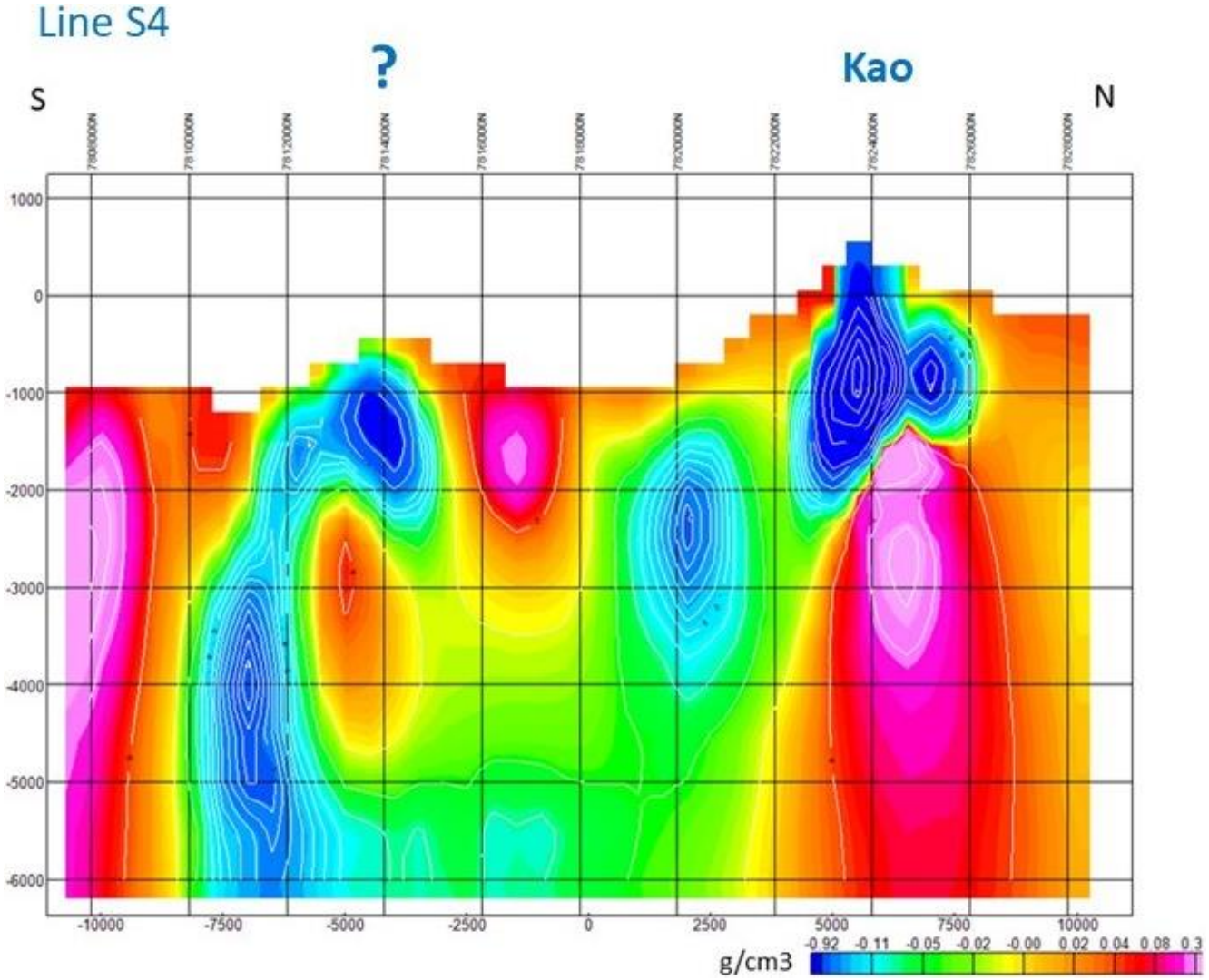

Figure 9 Cross-section S4 is located E of the toroidal structure (Figure 2) sampling a close, low-density region, and Kao Volcano to the N. The former feeds an unnamed volcanic structure whose summit is located at 500 m bsl, with a well-defined cone. The magmatic deposit feeding Kao Volcano is quite superficial and is connected to the broad, mid-density channel feeding the whole section. The color scale represents density contrast values relative to +2.67 g/cm^3

Cross-section S4 (Figure 2) does not intersect the Tofua structure; it runs in the N-S direction E of S3, crossing the SE portion of the Tofua structure and the NW portion of the Kao volcano. The purpose of this cross-section is to explore the characteristics of the gravity minimum that appears SE of the main Tofua anomaly; it reveals that a low-density channel rises vertically from the bottom of the cross-section to the surface feeding a volcanic cone whose summit lays 500 m bsl. A very surficial, low-density concentration under Kao volcano shows two minima at -800 m. Both structures appear to be fed by the same deep reservoir, below -6000 m, as suggested by the extent of the medium-density region between the two structures.

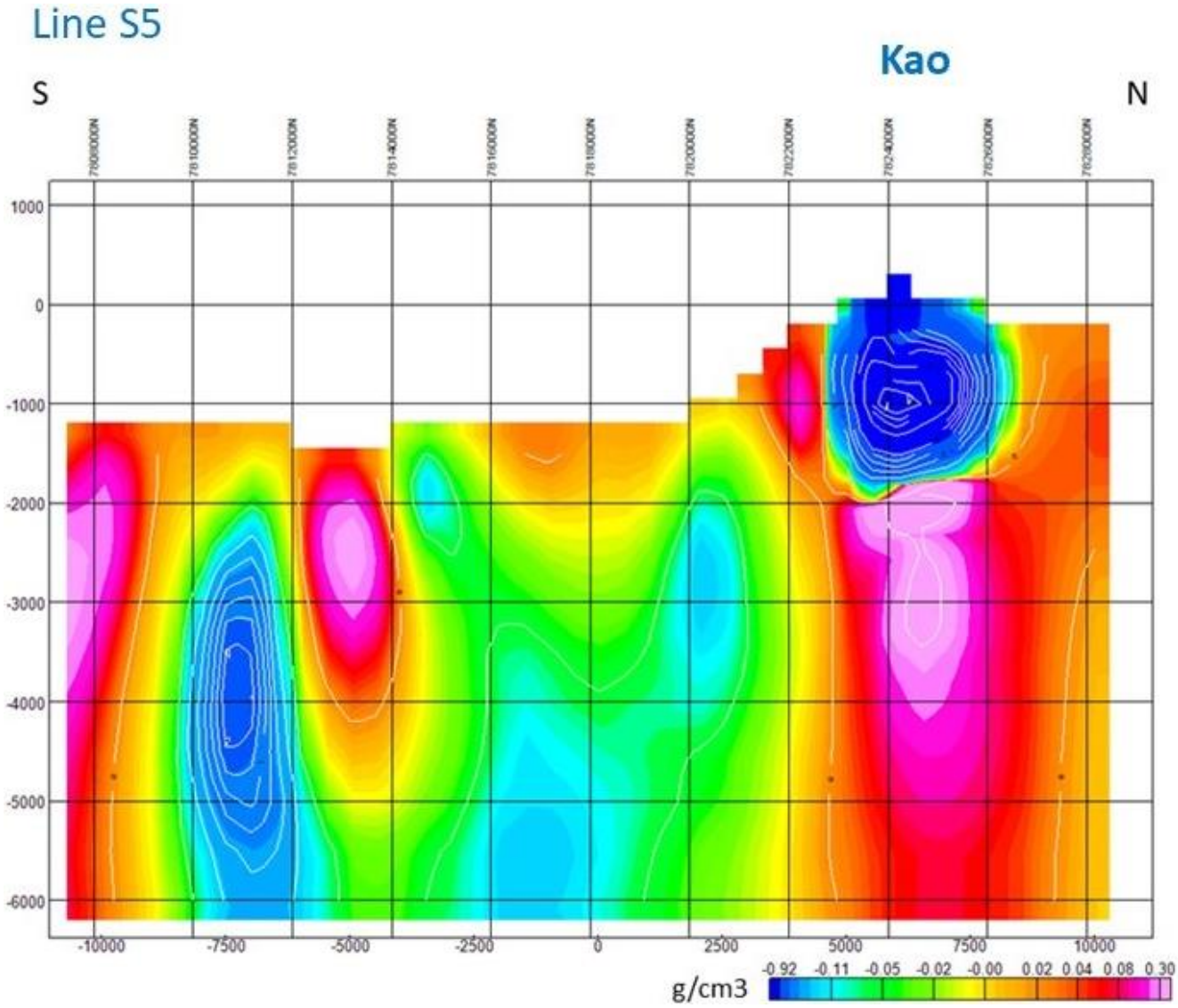

Figure 10 Cross-section S5 is located E of the toroidal structure (Figure 2) sampling Kao Volcano to the N. The two low-density minima observed in S4 under Kao volcano, coalesce here into a single, low-density chamber with a minimum at -1000 m, fully surrounded by high-density regions. The color scale represents density contrast values relative to +2.67 g/cm^3

The objective of cross-section S5 (Figure 2) which runs in the N-S direction E of S4, is to further explore Kao volcano's characteristics. The low-density anomaly is directly located in the upper portion of the volcanic structure, occupying most of its volume.; the minimum of this volcanic deposit is located at -1 km depth. From this low-density distribution, it would intuitively appear that Kao offers a greater eruptive probability than Tofua.

The vertical, low-density channel in the S portion persists but does not reach the surface. The large, medium-density region between the volcanoes remains; however, its direct connection with the low-density, Kao anomaly is no longer observed.

4 Discussion

The powerful eruption of the Hunga Tonga Hunga Ha'apai volcano (HTHH) on 15 January 2022, located 96 km SW of the Tofua volcano [10, 12, 23, 27, 39, 40], injected 10 percent of the whole water content of the stratosphere, reaching 53 km in altitude during the eruption [27, 43]. The most direct explanation for the production of this extraordinary, intense water vapor production is the interaction of volcano magmatic products with seawater, which in turn requires a large surface contact area to achieve the high evaporation rate required.

The volcanic interior of the HTHH volcano was explored from the gravity viewpoint [2] finding that instead of a magma chamber feeding a chimney, there was a disorderly distribution of low-density regions on the volcano's surface, identifying two areas, one of 12 km^2 on the W side of the structure and the other of 14 km^2 on the E side. In [2] also identified a low-density ring of density <2.26 g/cm^3, located between depths of -1190 and – 670 m which, following the model proposed in [9], was linked to the existence of ring fractures. Using also gravity analyses [25], the authors concurrently resolved that there is a complex, multi-reservoir magma system in the volcano, with two main, low-density reservoirs. If the toroidal deposit existed at some time in the HTHH volcano, as suggested by the findings in [2], we may speculate that a subsequent eruption, of the many experienced by this volcano, almost completely destroyed the torus, leaving only fragments circularly distributed in the region it occupied, which appear to be periodically reactivated.

With the present results, a possible explanation for the existence of these two areas in HTHH Volcano may follow the description in [9], arguing that a series of ring fractures occurred along with the collapse of the main cone in HTHH volcano. We submit that the ring fractures were exposed to the magma feeders, as is observed in the case of Tofua volcano (Figures 8 and 9), since they find a smaller resistance to the injection of the magmatic components, creating a deposit with a toroidal shape, similar to the one obtained for Tofua volcano.

If the assumption is correct, in the case of HTHH Volcano portions of the low-density toroidal deposit were scattered in chaotic patterns by the eruption, which when lumped together became the two, low-density regions reported above of 12 and 14 km^2. Considering that the low-density regions reported by these authors are mainly located within 2 km depth, and multiplying by the areas reported above, we obtain a volume of low-density materials of 52 km^3, that compares with the estimated volume for the torus of the Tofua volcano: 59 $km^{3.}$ The model presented here for the dispersion of the surficial, low-density regions of the HTHH Volcano would not appear viable without the discovery of the toroidal, magmatic deposit of Tofua Volcano. Although additional confirmation is required for its validation, this model provides a working platform for disciplines other than gravity, from which additional support can be obtained.

5 Conclusions

Here, we discovered a toroidal deposit associated with the Tofua volcanic structure, which we identify with the ring fracture zone created by the collapse of its magmatic chamber. Since it corresponds to a low-density region, we infer that the toroidal volume, weakened by the ring faults, was invaded by magmatic materials, resulting in the observed toroidal deposit. After confirming its structure and describing its characteristics, we proceeded to extend the structural analysis of the Tofua Volcano to the HTHH Volcano.

Identifying a toroidal magmatic deposit associated with a volcanic structure departs from the traditional concept of a magma chamber or magma deposit. Here we have confirmed its existence by analyzing the density distribution with depth of the 3D inverted gravity field, obtaining an isosurface from the 3D density distribution, and looking at various density cross-sections obtained from such distributions.

We link the toroidal, low-density distribution in the Tonga volcano with a possible, similar construct in the HTHH volcano; both structures are submarine volcanoes of the Tonga volcanic arc and both experienced caldera collapses. Since the spreading of low-density regions in the HTHH volcano will likely remain chaotic, and the volcano experiences repeated, explosive eruptions, a recurrence of the effects observed in the 2022 eruption can be expected. The possibility also exists that the Tofua volcano may experience an eruption that would destroy its toroidal deposit, perhaps reproducing the conditions prevailing at the HTHH volcano. Finally, the question arises of determining how common is, in structures with caldera collapses of the Tonga-Kermadec volcanic arc, the occurrence of toroidal magma deposits.

The analyses performed on Tofua and HTHH volcanoes, based on the inversion of high-resolution, satellite-derived gravity, has been previously applied to other volcanic structures, some reported here, and others reported elsewhere. The methodology can be applied to any volcanic structure where this type of data is available.

Acknowledgments

During development of this work, MC received support from Consejo Nacional de Ciencia y Tecnología (CONACYT), México. This study has been supported by IIMAS, UNAM; we acknowledge material support from both institutions. This research did not receive any specific grant from funding agencies in the public, commercial, or

not-for-profit sectors.

Availability Statement

The Bouguer anomaly data used here were obtained from http://ddfe.curtin.edu.au/gravitymodels/GGMplus/ (GGMplus, 2015). Processing of the data was made with the Oasis Montaj software, mainly for the 3D gravity to density inversion process; however, this is not the only code for performing 3D gravity inversions. Along with the gravity data, a topography/bathymetry digital elevation model is necessary, to perform the inversion. Once the data is inverted, the cross-sections can be readily obtained from the density model. The General Bathymetric Chart of the Oceans (GEBCO, 2021) provides freely available digital elevation models (DEMs) of the world's oceans, the pertinent ones were used in this investigation. The Chart of the Oceans can be obtained from [42]: https://www.gebco.net/data_and_products/gridded_bathymetry_data/#global.

The data that supports this work is preserved in repository: https://mega.nz/folder/btJCWbyB#k6i4SoE3v59ClbU3BXq6vg

References

[1] Alvarez, R., Yutsis, V., (2015). Southward Migration of Magmatic Activity in the Colima Volcanic Complex, Mexico: An Ongoing Process. International Journal of Geosciences, 6(9): 1077–1099. https://doi.org/10.4236/ijg.2015.69085

[2] Alvarez, R. and Camacho, M. (2023a). Plumbing System of Hunga Tonga Hunga Ha'apai Volcano. Journal of Earth Science, 34(3): 706–716. https://doi.org/10.1007/s12583-022-1792-0

[3] Alvarez, R. and Camacho, M. (2023b). Applying High-Resolution Gravity Analysis to Volcanic Plumbing Systems: The Case of Nevado De Toluca Volcano, Mexico. Transactions on Engineering and Computing Sciences, 11(4). 184-207. https://doi.org/10.14738/tecs.114.15392

[4] Alvarez, R., Camacho, M., & Rivera-Calderón, E. (2024). The Internal Structure of Paricutin and Tancítaro Volcanos, Mexico, From Rock Density Distributions. Transactions on Engineering and Computing Sciences, 12(2). 50-69. https://doi.org/10.14738/tecs.122.16645.

[5] Bauer, G. R. (1970) The geology of Tofua Island, Tonga. Pac Sci. 24: 333–350.

[6] Baker, P. E., Harris, P. G., Reay, A., 1971. The geology of Tofua Island, Tonga. Royal Society of New Zealand Bulletin 8, 67–79.

[7] Bryan, W. B., Stice, G. D., Ewart, A., (1972). Geology, Petrography, and Geochemistry of the Volcanic Islands of Tonga. Journal of Geophysical Research, 77(8): 1566 – 1585. https://doi.org/10.1029/jb077i008p01566

[8] Carvajal M, Sepúlveda I, Gubler A, Garreaud R (2022) Worldwide signature of the 2022 Tonga volcanic tsunami. Geophys Res Lett. https://doi.org/10.1029/2022GL098153

[9] Caulfield, J. T., Cronin, S. J., Turner, S. P., et al., (2011). Mafic Plinian Volcanism and Ignimbrite Emplacement at Tofua Volcano, Tonga. Bulletin of Volcanology, 73(9): 1259-1277. https://doi. org/10.1007/s00445-011-0477-9

[10] Clare et al., (2023). Fast and destructive density currents created by ocean-entering volcanic eruptions. Science 381, 1085–1092 (2023). https://doi.org/10.1126/science.adi3038

[11] Di Muro, A., Métrich, N., Vergani, D., Rosi, M., Armienti, P., Fougeroux, T., et al. (2014). The shallow plumbing system of Piton de la Fournaise Volcano (La Réunion Island, Indian Ocean) revealed by the major 2007 caldera-forming eruption. Journal of Petrology, 55(7), 1287–1315. https://doi.org/10.1093/petrology/egu025

[12] Donner, S., Steinberg, A., Lehr, J., Pilger, C., Hupe, P., et al., (2023). The January 2022 Hunga Volcano explosive eruption from the multi-technological perspective of CTBT monitoring. https://academic.oup.com/gji/advancearticle/doi.10.1093/gji/ggad204/7172861

[13] Forsberg, R. (1984), A study of terrain reductions, density anomalies and geophysical inversion methods in gravity field modelling, Report 355, Department of Geodetic Science and Surveying, Ohio State 783 University, Columbus.

[14] Guevara-Betancourt, R., et al., (2023) Insights into the plumbing system of Colima Volcanic Complex. Jour. Volcanol. Geothermal Res. 2022 433 (2023) 107711. https://doi.org/10.1016/j.jvolgeores.2022.107711

[15] Henley, RW, de Ronde, CEJ, Arculus, RJ, et al., (2023). The 15 January 2022 Hunga (Tonga) eruption: A gas-driven climatic explosion, Journal of Volcanology and Geothermal https://doi.org/j.jvolgeores.2024.108077

[16] Hildenbrand, T. G., Briesacher, A., Flanagan, G., et al., (2002). Rationale and Operational Plan to Upgrade the U. S Gravity Database. USGS Open File Report. Geology, Minerals, Energy and Geophysics Science Center, Moffett Field. 1–12. https://doi.org/10.3133/ofr02463

[17] Hirt, C. (2010), Prediction of vertical deflections from high-degree spherical harmonic synthesis and residual terrain model data, J. Geod., 84(3), 179-190. https://doi.org/10.1007/s00190-009-0354-x

[18] Hirt, C., Featherstone, W. E. and Marti, U. (2010), Combining EGM2008 and SRTM/DTM2006.0 residual terrain model data to improve quasigeoid computations in mountainous areas devoid of gravity data, J. Geod., 84(9): 327 557-567, https://doi.org/10.1007/s00190-010-0395-1

[19] Hirt, C., Claessens, S., Fecher, T., et al., (2013). New Ultra-high-Resolution Picture of Earth's Gravity Field. Geophysical Research Letters, 40(16): 4279–4283. https://doi.org/10.1002/grl.50838

[20] Inchin, P. A., Snively, J. B., Zettergren, M. D., Komjathy, A., Verkhoglyadova, O. P., & Tulasi Ram, S. (2020). Modeling of ionospheric responses to atmospheric acoustic and gravity waves driven by the 2015 Nepal Gorkha earthquake. Journal of Geophysical Research: Space Physics, 125. https://doi.org/10.1029/2019JA027200

[21] Kane, M. F., (1962). A Comprehensive System of Terrain Corrections Using a Digital Computer. Geophysics, 27(4): 455–462. https://doi.org/10.1190/1.1439044

[22] Komjathy, A., Galvan, D. A., Stephens, P., Butala, M. D., Akopian, V., Wilson, B., et al. (2012). Detecting ionospheric TEC perturbations caused by natural hazards using a global network of GPS receivers: The Tohoku case study. Earth Planets and Space, 64, 24. https://doi.org/10.5047/eps.2012.08.003

[23] Kusky, T. M. (2022). Déjà Vu: Might Future Eruptions of Hunga Tonga-Hunga Ha'apai Volcano be a Repeat of the Devastating Eruption of Santorini, Greece (1650 BC)? Journal of Earth Science, 33(2): 229–235. https://doi.org/10.1007/s12583-022-1624-2

[24] Legrand, D., Rouland, D., Frogneux, M., Carniel, R., Charley, D., Roult, G., & Robin, C. (2005). Interpretation of very long period tremors at Ambrym volcano, Vanuatu, as quasi-static displacement field related to two distinct magmatic sources. Geophysical Research Letters, 32(6), 1–5. https://doi.org/10.1029/2004GL021968

[25] Le Mével, H, Miller, CA, Ribó, M, and Cronin, SJ (2023). The magmatic system under Hunga volcano before and after the 15 January 2022 eruption. Science Advances ·December 2023. https://doi.org/10.1126/sciadv.adh3156

[26] Lipman, P. W. (1997). Subsidence of ash flow calderas: relation to caldera size and magma chamber geometry, Bull. Volcanol. 59 198218.

[27] Millán, L, Santee, ML, Lambert, A, Livesey, NJ, Werner, F, Schwartz, MJ, Pumphrey, HC, Manney, GL, Wang, Y, Su, H, Wu, L, Read, WG, Froidevaux, L. (2022). The Hunga Tonga-Hunga Ha'apai hydration of the stratosphere. Geophys. Res. Lett. 49, https://doi.org/10.1029/2022GL099381

[28] Moussallam, Y., Médard, E., Georgeais, G., Rose-koga, E., Koga, K., Pelletier, B., et al. (2021). How to turn off a lava lake? A petrological investigation of the 2018 intra-caldera and submarine eruptions of Ambrym volcano. Bulletin of Volcanology, 83(36), 1–19. https://doi.org/10.1007/s00445-021-01455-2

[29] Nagy, D., (1966). The Gravitational Attraction of a Right Rectangular Prism. Geophysics, 31(2): 362–371. https://doi.org/10.1190/1.1439779

[30] Poland, M., Miklius, A., & Montgomery-Brown, E. (2014). Magma supply, storage, and transport at shield-stage Hawaiian Volcanoes. In U.S. Geological Survey professional paper 1801, 2010 (pp. 1–52).

[31] Roche, O. & Druitt, T. H. (2001) Onset of caldera collapse during ignimbrite eruptions. Earth Planet Sci Lett 191: 191–202. https://doi.org/10.1016/S0012-821X(01)00428-9

[32] Scandone, R. (1990). Chaotic collapse of calderas, J. Volcanol. Geotherm. Res. 42, 285-302.

[33] Sandwell D, Garcia E, Soofi K, Wessel P, Chandler M, Smith WHF (2013). Toward 1-mGal accuracy in global marine gravity from CryoSat-2, Envisat, and Jason-1. Lead. Edge 32, 892–899 (2013).

[34] Sandwell, DT, Smith, WHF (2009) Global marine gravity from retracked Geosat and ERS-1 altimetry: Ridge segmentation versus spreading rate. J. Geophys. Res. Solid Earth. https://doi.org/10.1029/2008JB006008

[35] Shreve, T., Zhan, Y., Le Mével, H., Roman, D., & Moussallam, Y. (2023). Two distinct magma storage regions at Ambrym volcano detected by satellite geodesy. Geophysical Research Letters, 50. https://doi.org/10.1029/2023GL102925

[36] Smith, I. E. M., Price, R. C., (2006). The Tonga-Kermadec Arc and Havre-Lau Back-Arc System: Their Role in the Development of Tectonic and Magmatic Models for the Western Pacific. Journal of Volcanology and Geothermal Research, 156(3/4): 315-331. https://doi.org/10.1016/j.jvolgeores.2006.03.006

[37] Suryanata, PB, Bijaksana, S, Dahrin, D. et al., (2024). Subsurface structure of Bali Island inferred from magnetic and gravity modeling: new insights into volcanic activity and migration of volcanic centers. International Journal of Earth Sciences. https://doi.org/10.1007/s00531-024-02398-7

[38] Terry, JP, Goff, J, Winspear, N, Bongolan, VP, Fisher, S. (2022). Tonga volcanic eruption and tsunami, January 2022: globally the most significant opportunity to observe an explosive and tsunamigenic submarine eruption since AD 1883 Krakatau. Geoscience Letters. https://doi.org/10.1186/s40562-022-00232-z

[39] Themens, D. R., Watson, C., Žagar, N., et al., (2022). Global Propagation of Ionospheric Disturbances Associated with the 2022 Tonga Volcanic Eruption. Geophysical Research Letters, 49. https://doi.org/10.1029/2022gl098158

[40] Thurin, J. and Tape, C. (2023). Comparison of force and moment tensor estimations of subevents during the 2022 Hunga–Tonga submarine volcanic eruption. Geophys. J. Int. 235, 1959–1981 https://doi.org/10.1093/gji/ggad323

[41] Thurin, J., Tape, C., Modrak, R., (2022). Multi-Event Explosive Seismic Source for the 2022 Mw 6.3 Hunga Tonga Submarine Volcanic Eruption. The Seismic Record, 2(4): 217–226. https://doi.org/10.1785/0320220027

[42] Weatherall, P., Tozer, B., Arndt, J. E., et al., (2021). The GEBCO_2021 Grid a Continuous Terrain Model of the Global Oceans and Land. (2021-7-19) (2022-10-5). https://doi.org/10.5285/c6612cbe-50b3-0cffe053-6c86abc09f8f

[43] Yuen, D. A., Scruggs, M. A., Spera, F. J., et al. (2022). Under the Surface: Pressure-Induced Planetary-Scale Waves, Volcanic Lightning, and Gaseous Clouds Caused by the Submarine Eruption of Hunga Tonga-Hunga Ha'apai Volcano. Earthquake Research Advances, 2(3): 100134. https://doi.org/10.1016/j.eqrea.2022.100134

[44] Zettergren, M. D., and Snively, J. B. (2019). Latitude and longitude dependence of ionospheric TEC and magnetic perturbations from infrasonic-acoustic waves generated by strong seismic events. Geophysical Research Letters, 46, 1132–1140. https://doi.org/10.1029/2018GL081569